Available at
www.ElsevierComputerScience.com
POWERED BY SCIENCE DIRECT®

Signal Processing 86 (2006) 1737–1751

SIGNAL PROCESSING

www.elsevier.com/locate/sigpro

EEG–EMG coherence enhancement

Radoslav Bortel*, Pavel Sovka

Faculty of Electrical Engineering, Czech Technical University, Technicka 2, Prague, Czech Republic

Received 2 August 2004; received in revised form 7 July 2005
Available online 18 October 2005

Abstract

The paper introduces a new approach to the estimation of the EEG–EMG coherence, which is used to examine the functional connection between a human brain and muscles. A typical EEG–EMG coherence estimation, with a magnitude squared coherence (MSC) barely exceeding 0.15, is enhanced so that MSC reaches or even goes above 0.5. The proposed method is mathematically analyzed, and its properties are discussed. Additionally, the paper includes several EEG–EMG coherence analysis results, with MSC exceeding 0.5.

Keywords: Coherence; EEG; EMG

1. Introduction

The EEG–EMG coherence is usually used to examine a functional connection between a human brain and muscles [1–7]. It represents the relationship of the electroencephalogram (EEG), the record of brain activity and the electromyogram (EMG), the record of activity of a contracted muscle. The inspection of the relationship between these two signals provides information about the mechanism of the cortico-muscular interconnection. It helps to understand how a brain controls muscles [8,9], and also reflects movement disorders, e.g. Parkinson disease, cortical myoclonus or upper-limb dystonia (for more details refer to Appendix C).

Typically, magnitude squared coherence (MSC) of EEG and EMG is very low, normally around 0.1, barely exceeding 0.15, and not being distinguishable at all for some percentage of population. However, the recent research has shown that, with a proper pre-processing of an EEG signal, the EEG–EMG coherence can be enhanced so that its maximum MSC value exceeds 0.5 or at least is more distinguishable in the less favorable cases.

Typical EEG and EMG records are shown in Fig. 1. An average EEG record typically suffers from presence of a great amount of noise, which originates in brain functions, not related to the control process of the monitored muscle. Therefore, it is almost impossible to directly observe any relationship between EEG waveforms and spiky bursts typically appearing in the associated EMG. Consequently, the EEG–EMG MSC, example of which is shown in Fig. 2, is low.

Nevertheless, it was shown [1–7], that even though the EEG–EMG MSC is very small, it does represent a recognizable functional connection between a brain and muscular activity. Therefore,

*Corresponding author. Tel.: +420 224 352 158.
E-mail addresses: bortelr@feld.cvut.cz (R. Bortel), sovka@feld.cvut.cz (P. Sovka).

0165-1684/$ - see front matter © 2005 Elsevier B.V. All rights reserved.
doi:10.1016/j.sigpro.2005.09.011

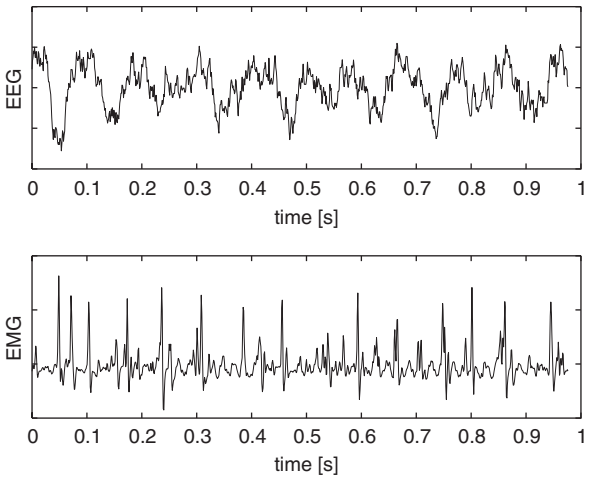

Fig. 1. Typical EEG and EMG waveforms.

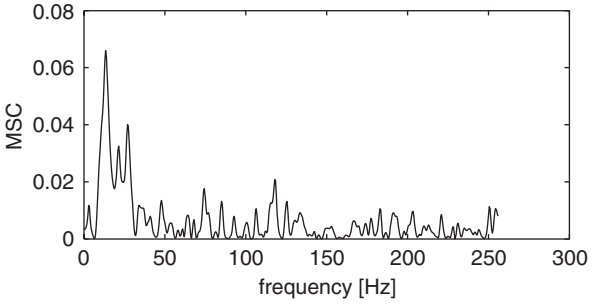

Fig. 2. Example of EEG and EMG MSC. As usual, its maximum does not exceed value of 0.1.

one could presume that in the EEG record there is a waveform, which corresponds to the actual drive of the muscle, and this waveform is strongly related to the EMG signal (i.e. the MSC of this waveform and the EMG signal is high). Hence, if this waveform was successfully extracted from EEG, its coherence with the corresponding EMG signal would increase significantly.

This paper proposes a method which purges an EEG signal of the waveforms uncorrelated to the muscular EMG activity, and keeps only the signal related to the activity in the muscle. Thus, this method increases the EEG–EMG MSC to the levels of 0.5 and higher, providing more sensitive tool for the EEG–EMG coherence analysis.

2. Currently used method of EEG–EMG coherence estimation

Currently, the EEG–EMG coherence is estimated in the following manner.

First, the EEG signal, measured by several electrodes on the head of an examined subject, is spatially filtered, so that the signal from the electrode sensing activity in the sensimotor cortex is purged of any activity coming from completely different parts of the brain.

Additionally, the EMG signal, measured by two electrodes placed over a muscle performing a constant contraction, undergoes a simple pre-processing of rectification.

Next, the coherence function is computed. EEG, denoted as $u[n]$, and the rectified EMG, denoted as $v[n]$, are segmented into L segments, and then the coherence is estimated (e.g. see [3]) according to

$$\widehat{\gamma}_{uv}(\Omega)=\frac{(1/L)\sum_{l=1}^{L}U_l^*(\Omega)V_l(\Omega)}{\sqrt{(1/L)\sum_{l=1}^{L}|U_l(\Omega)|^2\cdot(1/L)\sum_{l=1}^{L}|V_l(\Omega)|^2}}, \tag{1}$$

where $\widehat{\gamma}_{uv}(\Omega)$ is the estimate of the coherence function of the signals ($|\widehat{\gamma}_{uv}(\Omega)|^2$ is magnitude squared coherence—MSC), $u[n]$ and $v[n]$, $U_l(\Omega)$ is the spectrum of $u[n]$ in the lth segment, $V_l(\Omega)$ is the spectrum of $v[n]$ in the lth segment, and the asterisk denotes the complex conjugation.

Last, the resulting MSC needs to be decided whether it is significant enough to indicate any functional connection between the sensimotor cortex and the monitored muscle. Several approaches to determine MSC significance were used so far. In this paper, a method adopted from [6] will be used. This method is based on a comparison of the resulting MSC with an MSC computed from the EEG and EMG signals time shifted so that any true coherence is gone. The MSC of the time shifted signals consists of a random coherence only; therefore, it is used to compute a floor, exceeding of which makes the original MSC significant. This floor, termed as the confidence limit, is computed as a value, under which lies 95% of the random MSC. If the original MSC clearly exceeds this confidence limit, it is considered to be significant, and proves functional connection between the EEG and EMG activity.

The coherence computed by the described approach, however, suffers from a great amount of noise, which is present in the EEG signal due to our inability to filter out all of the brain signals not related to the activity in the monitored muscle (the spatial filtering of the signals from EEG electrodes is far too insufficient to extract just one signal from a brain). Consequently, the coherence mostly does

not exceed the value of 0.15, and sometimes no significant coherence is found.

Therefore, an effort was spent to find a way to suppress the parasitic signals in EEG which are not related to the EMG activity. One way how to purge the EEG signal is proposed in Section 3.

3. Proposed methods

The proposed method of a EEG–EMG coherence computation uses the same computational steps as the previously described method; additionally, it performs some more advanced EEG pre-processing, which purges EEG signal of the waveforms not related to the EMG activity.

3.1. Pre-processing

The idea of this pre-processing is to search for a signal which repeatedly occurs in the neighborhood of the spiky bursts typically occurring in EMG. We suppose that if there is a signal driving EMG bursts present in EEG, then this signal should approximately repeat itself in the neighborhood of the EMG bursts. On the other hand, if instead of the driving signal only noise is present, this noise is uncorrelated to the EMG activity, and so in the bursts' neighborhood is always different. Therefore, the pre-processing will try to find the signal which repeats itself around the EMG bursts, and will suppress all the noises which do not seem to be related to the EMG bursts.

This can be done as follows.

First, the positions of the EMG bursts needs to be found. It is possible to find the bursts in many ways; however, it will be shown later that this step is not really necessary, and is included only for explanatory reasons, so at this point we will satisfy with an assumption that the EMG bursts have been found somehow. An illustration of what the found EMG bursts look like is in Fig. 3, where arrows indicate positions of recognized EMG bursts.

Next, the positions of the found EMG bursts are recorded into a new signal $\widetilde{v}[n]$, which has the value of one for index n, where a burst in the EMG signal has occurred, and zero otherwis4

$$\widetilde{v}[n] = \begin{cases} 1 & \text{if burst has occured at position } n, \\ 0 & \text{otherwise.} \end{cases} \tag{2}$$

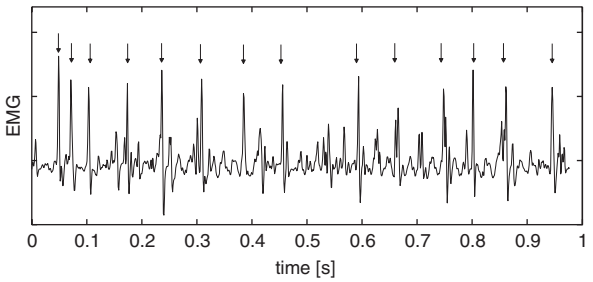

Fig. 3. Detection of bursts in EMG signal. The EMG bursts are indicated with arrows.

Further, again just for explanatory reasons, it will be supposed that the only useful information in EMG are the found bursts. Therefore, at least for now, the original rectified EMG signal $v[n]$ will be replaced with the newly constructed $\widetilde{v}[n]$, in which the bursts are contained as unity pulses.

Next, $\widetilde{v}[n]$ will be used to extract those EEG samples which are supposed to approximately repeat themselves in case a noise free driving signal is present in EEG. These repeating EEG samples should have a constant relative position towards the bursts in EMG (or in other words, they precede or lag behind the EMG bursts by a constant number of sample indexes), and so they can be extracted from EEG by multiplying it with a time shifted $\widetilde{v}[n]$ (limits of the time shift $-K, K$ will be determined later)

$$\widetilde{u}[n,k] = u[n] \cdot \widetilde{v}[n-k], \quad k = -K, \ldots, K. \tag{3}$$

The resulting system of sequences $\widetilde{u}[n,k]$ contains the original EEG data only on those positions, where $\widetilde{v}[n-k]$ is unity—that is on the positions which precede or lag the detected EMG bursts by k samples. The other positions will be zero. Thus $\widetilde{u}[n,k]$ for k constant will contain exactly those samples which should repeat themselves in case EEG contains only a noise free driving signal.

With random noise present, however, the extracted samples will be scattered. Therefore, to find the repeating contributions of driving signal, the extracted values $\widetilde{u}[n,k]$, k constant, will be searched for any average trend. This will be done through computing a moving average of $\widetilde{u}[n,k]$ according to

$$\begin{aligned} \{\widetilde{u}[n,k]\}_{\mathrm{av}} &= \sum_{m=-M}^{M} \widetilde{u}[n-m,k]b[m] \\ &= \widetilde{u}[n,k] * b[n], \quad n = 1, \ldots, N, \end{aligned} \tag{4}$$

where $\{\widetilde{u}[n,k]\}_{\mathrm{av}}$ denotes the averaged signal, $b[n]$ is a symmetric window of $2M+1$ weights with the

center of symmetry in $n = 0$,[1] N is the length of $u[n]$, and * stands for a convolution. Thus, this procedure computes the average values from the samples selected by the window $b[n]$ sliding along $\widetilde{u}[n,k]$, approximating the driving signal of the EMG bursts.

The result of the moving average (4) is affected by the non-zero values of $\widetilde{u}[n,k]$ only; the values zeroed by (3) have no effect on the result. However, after applying (4), all the samples in $\{\widetilde{u}[n,k]\}_{\mathrm{av}}$ will generally be non-zero. This is rather inconvenient for the further aim to reassemble the system of sequences $\{\widetilde{u}[n,k]\}_{\mathrm{av}}$, $k = -K,\ldots,K$ into a one resulting sequence. Therefore, in $\{\widetilde{u}[n,k]\}_{\mathrm{av}}$ the non-zero values will be kept only on the positions which were non-zero originally in $\widetilde{u}[n,k]$. This means to apply the extraction process (3) again

$$\widetilde{\{\widetilde{u}[n,k]\}_{\mathrm{av}}} = \{\widetilde{u}[n,k]\}_{\mathrm{av}} \cdot \widetilde{v}[n-k], \quad k = -K,\ldots,K. \tag{5}$$

Now the last step will be to finally reassemble the sequences $\widetilde{\{\widetilde{u}[n,k]\}_{\mathrm{av}}}$, $k = -K,\ldots,K$, which at this point contain the averaged values extracted from EEG. This can be done by just adding these sequences together, while properly weighing them by some coefficients a_k (the coefficients a_k can simply be ones, but the further examination of the resulting formula will show a better choice)

$$u'[n] = \sum_{k=-K}^{K} a_k \widetilde{\{\widetilde{u}[n,k]\}_{\mathrm{av}}}. \tag{6}$$

To obtain the final result (3)–(5) are substituted into (6), yielding

$$u'[n] = \sum_{k=-K}^{K} a_k((u[n]\widetilde{v}[n-k]) * b[n])\widetilde{v}[n-k]. \tag{7}$$

Formula (7) is finally usable for the pre-processing of the EEG signal. If a coherence of signals $u'[n]$ and $\widetilde{v}[n]$ was computed, it might provide some nice results of coherence, with MSC exceeding 0.5. However, since the following examination of formula (7) needs no assumption on the signal $\widetilde{v}[n]$, it appears that $\widetilde{v}[n]$ can be any signal and not only the one with unity pulses at the positions of the EMG bursts. Therefore, it is possible to conveniently replace $\widetilde{v}[n]$ with the original EMG signal $v[n]$, which according to experiments seems to provide the best results. Hence, formula (7) can be rewritten as

$$u'[n] = \sum_{k=-K}^{K} a_k((u[n] \cdot v[n-k]) * b[n])v[n-k]. \tag{8}$$

Furthermore, the mentioned steps of finding the bursts in EMG and replacing of $v[n]$ with $\widetilde{v}[n]$ are no longer necessary.

3.2. Coherence analysis of pre-processed signals

In this section the coherence of the pre-processed EEG signal $u'[n]$ and the rectified EMG signal $v[n]$ will be examined. To do this $u'[n]$ and $v[n]$ first need to be segmented into $u'_l[n]$ and $v_l[n]$, where l is an index of a segment. Then, the Fourier transforms of the signals in each segment needs to be found.

3.2.1. Fourier transform of pre-processed signals

The Fourier transform of $v_l[n]$ is straightforward

$$V_l(\Omega) = \mathscr{F}\{v_l[n]\}, \tag{9}$$

where $\mathscr{F}\{.\}$ denotes the Fourier transform.

The Fourier transform of $u'_l[n]$ can be found transforming the pre-processing formula (8), but before doing so, it is convenient to rearrange (8) slightly.

First, the expression $(u[n] \cdot v[n-k]) * b[n]$ in (8) actually represents the estimate of the cross-correlation function of $v[n]$ and $u[n]$ computed from samples $n-M,\ldots,n+M$ [10] (the span of these limits is given by the length $2M+1$ of the window formed by the weights $b[n]$)

$$\begin{aligned}\widehat{R}_{vun}[k] = \widehat{R}_{uvn}[-k] &= (u[n] \cdot v[n-k]) * b[n] \\ &= \sum_{m=n-M}^{n+M} u[m]v[m-k]\ b[n-m], \\ &\quad n = M+K,\ldots,N-M-K,\end{aligned} \tag{10}$$

where $\widehat{R}_{vun}[k]$ is the cross-correlation estimate, and N is the length of the sequences $u[n]$ and $v[n]$.

For further analysis it is important to notice, that the precision of the estimate $\widehat{R}_{vun}[k]$, for $|k|$ small, improves with an increasing number of samples this estimate is computed from [11]—that is, it improves with a growing length $2M+1$ of the window $b[n]$.

Additionally, since the final result will contain the Fourier transform of $\widehat{R}_{uvn}[k]$, we will investigate the effect of window $b[n]$ in the spectral domain. The fourier transform of (10) is

$$\mathscr{F}\{\widehat{R}_{uvn}[k]\} = V^*(\Omega) \cdot (U(\Omega) * (B^*(\Omega)\mathrm{e}^{-\mathrm{j}n\Omega})), \tag{11}$$

[1] This setup ensures that no time/phase shifts are introduced into the resulting signal.

where $U(\Omega)=\mathscr{F}\{u[n]\}$, $V(\Omega)=\mathscr{F}\{v[n]\}$ and $B(\Omega)=\mathscr{F}\{b[n]\}$. It seems that window $b[n]$ can cause some spectral leakage as its Fourier transform convolves with $U(\Omega)$. To minimize this, we suggest to use a low leakage window, e.g. the Hamming window (Appendix E shows that choosing a different low leakage window does not have any significant effect on the resulting coherence).

Now, substitution of (10) into (8) provides

$$u'[n]=\sum_{k=-K}^{K} a_k\cdot\widehat{R}_{vun}[k]\cdot v[n-k]. \tag{12}$$

Next, to simplify the Fourier transform of (12), the cross-correlation estimates $\widehat{R}_{vun}[k]$ for all n within one segment l will be approximated by just one cross correlation estimate $\widehat{R}_{vul}[k]$. This is possible because of two reasons. First, within short segments, the EEG signal can be considered stationary, and so the true cross-correlation should be constant there, which suggests an approximately constant cross-correlation estimate $\widehat{R}_{vun}[k]$. Second, for good results (according to our experimental assessment) it is necessary to compute the cross-correlation estimate $\widehat{R}_{vun}[k]$ from more samples than 15 times the number of samples in a segment. Thus, with n constrained within one segment, n changes only a little compared to the length $2M+1$ of the intervals $n-M,\ldots,n+M$, which $\widehat{R}_{vun}[k]$ are computed from. Hence, with n within one segment, the intervals $n-M,\ldots,n+M$ contains a lot of same samples, and $\widehat{R}_{vun}[k]$ are dependent and similar. Therefore, in each segment, $\widehat{R}_{vun}[k]$ will be replaced by just one estimate $\widehat{R}_{vul}[k]$ given by

$$\widehat{R}_{vul}[k]=\widehat{R}_{vun}[k]\quad \text{where } n \text{ is an index amidst the segment } l. \tag{13}$$

Using (13), (12) changes into approximation of $u'[n]$

$$u'_l[n]\doteq\sum_{k=-K}^{K} a_k\cdot\widehat{R}_{vul}[k]\cdot v[n-k]\quad \text{for } n \text{ within the segment } l. \tag{14}$$

Applying the Fourier transform yields

$$U'_l(\Omega)\doteq\sum_{k=-K}^{K} a_k\cdot\widehat{R}_{vul}[k]\cdot V_l(\Omega)\cdot \mathrm{e}^{-\mathrm{j}\Omega k}. \tag{15}$$

Next, since $\mathrm{e}^{-\mathrm{j}\Omega k}$ is the Fourier transform core, and $a_k\cdot\widehat{R}_{vul}[k]$ is the weighted cross-correlation function of $u_l[k]$ and $v_l[k]$, it is possible to transform (15) to

$$U'_l(\Omega)\doteq\widehat{S}_{vul}(\Omega)\cdot V_l(\Omega), \tag{16}$$

where $\widehat{S}_{vul}(\Omega)$ is a smoothed estimate of the cross-spectral density of $u_l[k]$ and $v_l[k]$

$$\widehat{S}_{vul}(\Omega)=\mathscr{F}\{a_k\cdot\widehat{R}_{vul}[k]\}. \tag{17}$$

Even though (16) already is a Fourier transform of $u'_l[k]$, to examine EEG–EMG correlation more closely, it is suitable to rearrange (16) so that the properties of the transfer path between EEG and EMG will be clearly shown. This can be accomplished [12] by expressing the cross-spectrum estimate $\widehat{S}_{vu}(\Omega)$ in terms of the auto-spectral density estimate, given as

$$S_v(\Omega)=E[|V_l|^2(\Omega)], \tag{18}$$

and the complex transfer function $\widehat{H}_l(\Omega)$ which estimates the transfer path from $v_l[k]$ to $u_l[k]$

$$\widehat{S}_{vul}(\Omega)=\widehat{H}_l(\Omega)\cdot S_v(\Omega). \tag{19}$$

Substituting (19) into (16) yields the sought Fourier transform of $u'_l[k]$ suitable for further analysis

$$U'_l(\Omega)\doteq S_v(\Omega)\cdot\widehat{H}_l(\Omega)\cdot V_l(\Omega). \tag{20}$$

Additionally, at this point it is possible to decide the values of the coefficients a_k. Since the window a_k multiplies with $\widehat{R}_{uvl}[k]$ in the time domain, in the spectral domain the window a_k will cause spectral smearing and spectral leakage. Therefore, we suggest using a low leakage window with acceptable spectral smearing, e.g. Hamming window.

3.2.2. Interpretation of pre-processing

With the Fourier transform of $u'_l[k]$ found, it is possible to interpret the pre-processing results. According to (20) rearranged into

$$U'_l(\Omega)\cdot\frac{1}{\widehat{H}_l(\Omega)}\doteq V_l(\Omega)\cdot S_v(\Omega), \tag{21}$$

$u'_l[n]$ is the signal which has created $v_l[n]$ linearly transformed by $S_v(\Omega)$ through a system with the transfer function $1/\widehat{H}_l(\Omega)$. Because $\widehat{H}_l(\Omega)$ estimates the transfer path from the EMG signal $v_l[n]$ to the EEG signal $u_l[n]$ in the segment l, the inverse transfer function $1/\widehat{H}_l(\Omega)$ in a certain way estimates the transfer path from EEG to EMG. Therefore, $u'_l[k]$ can be interpreted as an approximation of the sought driving signal of the bursts in EMG (additionally, $u'_l[k]$ is affected by the linear transformation by $S_v(\Omega)$, which, however, owing to its linearity, has no influence on the resulting coherence).

Also it could be noted that the way of estimation of the transfer function $\widehat{H}(\Omega)$ and expressions (20) and (21) resemble the Wiener filtration [12].

3.2.3. Noise suppression of pre-processing

Expression (20) can further explain how the proposed pre-processing suppresses noise in the EEG signal $u[n]$. If $u[n]$ consists of a useful signal $u_S[n]$ and a noise $u_N[n]$, which is not correlated with $u_S[n]$

$$u[n] = u_S[n] + u_N[n], \tag{22}$$

then substituting (22) into the pre-processing formula (8) yields

$$u'[n] = \sum_{k=-K}^{K} a_k((u_S[n] \cdot v[n-k]) * b[n])v[n-k] + \sum_{k=-K}^{K} a_k((u_N[n] \cdot v[n-k]) * b[n])v[n-k]. \tag{23}$$

Which, applying the Fourier transform (20), provides

$$U'_l(\Omega) \doteq S_v(\Omega) \cdot \widehat{H}_{Sl}(\Omega) \cdot V_l(\Omega) + S_v(\Omega) \cdot \widehat{H}_{Nl}(\Omega) \cdot V_l(\Omega), \tag{24}$$

where $\widehat{H}_{Sl}(\Omega)$ is an estimate of the transfer function between $v_l[n]$, and $u_{Sl}[n]$ and $\widehat{H}_{Nl}(\Omega)$ is an estimate of the transfer function between $v_l[n]$ and $u_{Nl}[n]$. The second estimate $\widehat{H}_{Nl}(\Omega)$, however, will be close to zero, because the noise $u_N[n]$ is not correlated with $v[n]$. Therefore, $U'_l(\Omega)$ and $u'[n]$ will approach to

$$U'_l(\Omega) \to S_v(\Omega) \cdot \widehat{H}_{Sl}(\Omega) \cdot V_l(\Omega), \tag{25}$$

$$u'[n] \to \sum_{k=-K}^{K} a_k((u_S[n] \cdot v[n-k]) * b[n])v[n-k]. \tag{26}$$

So the pre-processed signal $u'[n]$ will not be affected by the noise in the EEG signal $u[n]$. This, of course, has a beneficial influence on the resulting coherence, as will be shown in the next section.

3.2.4. Coherence of pre-processed signals

With the Fourier transform of $u'_l[n]$ and $v_l[n]$ found, it is possible to examine their coherence function $\gamma_{u'v}(\Omega)$, defined as

$$\gamma_{u'v}(\Omega) = \frac{S_{u'v}(\Omega)}{\sqrt{S_{u'}(\Omega) \cdot S_v(\Omega)}}, \tag{27}$$

where $S_{u'v}(\Omega)$ is the cross-spectral density of $u'[n]$ and $v[n]$, $S'_u(\Omega)$ is the auto-spectral density of $u'[n]$, and $S_v(\Omega)$ is the auto-spectral density of $v[n]$.

Assuming that $u[n]$ and $v[n]$ are stationary and ergodic, the coherence function (27) can by estimated as [13,14]

$$\widehat{\gamma}_{u'v}(\Omega) = \frac{(1/L)\sum_{l=1}^{L} U'^{*}_l(\Omega)V_l(\Omega)}{\sqrt{(1/L)\sum_{l=1}^{L}|U'_l(\Omega)|^2 \cdot (1/L)\sum_{l=1}^{L}|V_l(\Omega)|^2}}. \tag{28}$$

Substituting (20) gives a coherence function estimate

$$\widehat{\gamma}_{u'v}(\Omega) \doteq \frac{(1/L)\sum_{l=1}^{L} S_v(\Omega) \cdot \widehat{H}^{*}_l(\Omega) \cdot V^{*}_l(\Omega) \cdot V_l(\Omega)}{\sqrt{(1/L)\sum_{l=1}^{L}|S_v(\Omega) \cdot \widehat{H}_l(\Omega) \cdot V_l(\Omega)|^2 \cdot (1/L)\sum_{l=1}^{L}|V_l(\Omega)|^2}}. \tag{29}$$

Owing to the ergodicity of $u[n]$ and $v[n]$, the sums in (29) can be asymptotically (i.e. for L large) estimated with the expected values of their arguments, and so the entire expression (29) can be asymptotically estimated as

$$\widehat{\gamma}_{u'v}(\Omega) \to \frac{\Sigma_1}{\sqrt{\Sigma_2 \cdot \Sigma_3}}, \tag{30}$$

where Σ_1, Σ_2 and Σ_3 are the expected values of the arguments of the sums in (29)

$$\Sigma_1 = E[S_v(\Omega) \cdot \widehat{H}^{*}_l(\Omega) \cdot V^{*}_l(\Omega) \cdot V_l(\Omega)] = S_v(\Omega) \cdot E[\widehat{H}^{*}_l(\Omega) \cdot |V_l(\Omega)|^2], \tag{31}$$

$$\Sigma_2 = E[|S_v(\Omega) \cdot \widehat{H}_l(\Omega) \cdot V_l(\Omega)|^2] = S_v^2(\Omega) \cdot E[|\widehat{H}_l(\Omega)|^2 \cdot |V_l(\Omega)|^2], \tag{32}$$

$$\Sigma_3 = E[|V_l(\Omega)|^2] = S_v(\Omega). \tag{33}$$

First, let us investigate the case when $u[n]$ and $v[n]$ are independent. Expression (31), as shown in Appendix A, can be conveniently expressed in terms of $u[n]$ and $v[n]$ as

$$\Sigma_1 = S_v(\Omega) \cdot E[\widehat{H}^{*}_l(\Omega) \cdot |V_l(\Omega)|^2] = A^{*}(\Omega) * \sum_{m=n-M}^{n+M} (b[n-m] \cdot E[u[m] \cdot \mathscr{F}\{v[m+k]\} \cdot |V_l(\Omega)|^2]), \tag{34}$$

where $A(\Omega)$ is the Fourier transform of the sequence a_k. Owing to the independence of $u[n]$ and $v[n]$, the expected value operator in (34) can be divided into

two parts

$$A^*(\Omega) * \sum_{m=n-M}^{n+M} (b[n-m] \cdot E[u[m]] \cdot E[\mathscr{F}\{v[m+k]\} \cdot |V_l(\Omega)|^2]). \quad (35)$$

And because the average value of $u[n]$ is zero (if it is not, any DC component should be cancelled), its ergodicity suggests $E[u[n]] = 0$, and so the whole expression (35) is zero. Therefore, the numerator of (30) is zero as well.

Moreover, since expressions (32) and (33) are generally non-zero (except of the degenerated case of $v[n] = 0$) the denominator of (30) is non-zero, too. Thus the entire expression (30) is zero.

Therefore, if $v[n]$ and $u[n]$ are independent, and the number of segments L is large enough to estimate the sums in (29) by the mean values of their arguments, $\widehat{\gamma}_{u'v}(\Omega)$ goes to zero.

Now, let us investigate the case when $u[n]$ and $v[n]$ are somehow dependent. To express the coherence function estimate (30) in an analyzable way, it is convenient to express the spectral characteristic estimates in terms of their expected values and the expected value estimate errors, some of which will lessen and vanish as the estimates of the expected values get more precise. Specifically, it is suitable to express $\widehat{S}_{uvl}(\Omega)$ and $|V_l(\Omega)|^2$ like this

$$\widehat{S}_{uvl}(\Omega) = E[\widehat{S}_{uv}(\Omega)] + e_{S_{uvl}}(\Omega) = S_{uv}(\Omega) + e_{S_{uv}l}(\Omega), \quad (36)$$

$$|V_l(\Omega)|^2 = E[|V_l(\Omega)|^2] + e_{Vl}(\Omega) = S_v(\Omega) + e_{Vl}(\Omega), \quad (37)$$

where $S_{uv}(\Omega)$ and $S_v(\Omega)$ are the expected values of $\widehat{S}_{uv}(\Omega)$ and $|V_l(\Omega)|^2$, respectively, and $e_{S_{uvl}}(\Omega)$ and $e_{Vl}(\Omega)$ are errors of $\widehat{S}_{uv}(\Omega)$ and $|V_l(\Omega)|^2$ used as estimates of their expected values. Also it is convenient to denote the expected value of $\widehat{H}_l(\Omega)$,

$$H(\Omega) = E[\widehat{H}_l(\Omega)]. \quad (38)$$

In these terms, as shown in Appendix B, the expressions for Σ_1 (31) and Σ_2 (32) can be rewritten into new forms (B.2) and (B.5), substitution of which into the coherence estimate (30) yields

$$\widehat{\gamma}_{u'v}(\Omega) \to \frac{\Sigma_1}{\sqrt{\Sigma_2 \cdot \Sigma_3}} = \frac{S_v^2(\Omega) \cdot H^*(\Omega) + E[e_{S_{uvl}}(\Omega) \cdot e_{Vl}(\Omega)]}{\sqrt{\Sigma_2 \cdot \Sigma_3}}, \quad (39)$$

where the expression in the denominator is

$$\Sigma_2 \cdot \Sigma_3 = (S_v^3(\Omega) \cdot |H(\Omega)|^2 + 2\Re\{S_{uv}(\Omega)E[e^*_{S_{uvl}}(\Omega) \cdot e_{Vl}(\Omega)]\} + S_v(\Omega)E[|e_{S_{uvl}}(\Omega)|^2] + E[e_{Vl}(\Omega) \cdot |e_{S_{uvl}}(\Omega)|^2]) \cdot S_v(\Omega). \quad (40)$$

When $v[n]$ and $u[n]$ are not independent, with a growing precision of the estimate $\widehat{S}_{uvl}(\Omega)$, its expected value estimate error $e_{S_{uvl}}(\Omega)$ is decreasing, and consequently all the mean values in the (39) which contain $e_{S_{uvl}}(\Omega)$ are getting smaller and negligible. Therefore, as precision of $\widehat{S}_{uvl}(\Omega)$ increases, the coherence function estimate $\widehat{\gamma}_{u'v}$ approaches to

$$\widehat{\gamma}_{u'v} \to \frac{S_v^2(\Omega) \cdot H^*(\Omega)}{\sqrt{S_v^4(\Omega)|H(\Omega)|^2}} = \frac{H^*(\Omega)}{|H(\Omega)|} = 1 \cdot \mathrm{e}^{-\mathrm{j}\phi_{H(\Omega)}}. \quad (41)$$

The precision of the estimate $\widehat{S}_{uvl}(\Omega)$ improves with the precision of $\widehat{R}_{vul}[k]$, which increases with a growing length $2M + 1$ of the window $b[n]$.

In conclusion, if the number of segments L and the length $2M + 1$ of the window $b[n]$ is sufficiently large, $\widehat{\gamma}_{u'v}(\Omega)$ approaches to the following:

$\widehat{\gamma}_{u'v}(\Omega) \to 0$ for $v[n], u[n]$ independent (i.e. no EEG−EMG functional connection), (42)

$\widehat{\gamma}_{u'v}(\Omega) \to 1 \cdot \mathrm{e}^{-\mathrm{j}\phi_{H(\Omega)}}$ for $v[n], u[n]$ somehow correlated (i.e. the functional connection exists). (43)

While (42) is a completely normal behavior of a coherence function of any two independent signals, (43) is an enhanced behavior, arising due to the pre-processing of the signals.

3.3. Proposed method summary

The proposed method should be used as follows: first, recorded EEG data are spatially filtered, while recorded EMG is rectified. Next, the EEG signal associated with the electrode placed over the sensimotor cortex contralateral to the contracted muscle is pre-processed with (8). Then, using the pre-processed EEG and the rectified EMG, the coherence is computed with (28). Last, to compute a

confidence limit, the coherence of the time shifted EEG and EMG signals is computed in the same way,[2] estimating the confidence limit as a value, under which lies 95% of the coherence of the time shifted signals.[3]

The parameters of the pre-processing should be chosen according to the following guidelines.

First, the longer the window $b[n]$, the more distinct is the coherence at the frequencies, where EEG and EMG are dependent. The length of $b[n]$, however, should be much less than the length of the EEG record. Making $b[n]$ too long, would decrease the number of degrees of freedom of the coherence estimate, increasing its bias error. During practical tests on data sequences 2.5 min long ($\sim 77 \cdot 10^3$ samples; sampled at 512 Hz), making $b[n]$ the Hamming window with the length of 4000–5000 samples ($\sim$ 7.8 s or $\sim$ 9.8 s, respectively) proved to work fine.

Second, the sequence a_k should be the Hamming window long enough to provide a sufficient frequency resolution when used for weighing of a correlation function prior to its Fourier transform. For example, it should be at least 0.5 s long to provide the frequency resolution of 2 Hz.

4. Results

The proposed method was tested on a number of EEG and EMG data records, measured during a constant isometric contraction of an index finger (12 individuals were holding three different weights). Each contraction was 2.5 min. long, sampled at 512 Hz ($77 \cdot 10^3$ samples per measurement).

EEG was recorded from 82 scalp locations covering frontal, central, parietal and temporal scalp regions. The electrodes were positioned in a rectangular grid with spacing, approximately, 2.5 cm. Recorded data were spatially filtered [17] to eliminate current smearing caused by conducting layers of a head.

For the EEG–EMG coherence computation, we used EEG records from the electrodes positioned over a primary sensimotor area contralateral to the contracted muscle (the primary sensimotor area is involved in movement control, hence its EEG record is expected to be correlated with the EMG record of the contracted muscle). When more than one electrode demonstrated a significant EEG–EMG MSC, the electrode with the strongest MSC was chosen.

EMG was recorded using bipolar electrodes positioned over muscle extensor indicis longus, which is in charge extension of an index finger.

Parameters of the pre-processing were: $b[n]$ was the Hamming window of the length $2M + 1 = 5001$ ($\sim$9.8 s), and a_k was the Hamming window with the length $2K + 1 = 201$ ($\sim$0.4 s).

For the coherence computation, the signals were segmented into non-overlapping segments of 256 samples ($\sim$0.5 s).

The confidence limit was estimated from the MSC of EEG and EMG signals time shifted by 1000 samples ($\sim$1.95 s).

Some of the resulting MSCs are shown in Fig. 4. Each row in Fig. 4 shows results of one set of the EEG–EMG data. The first in each row there is the enhanced coherence function (its magnitude squared value), computed from the EEG and EMG signals pre-processed as proposed. In the middle column there is the original MSC computed in a common way without the proposed pre-processing (limits of the y-axis here are the same as for the enhanced coherence to show how small the original EEG–EMG MSC actually is). In the most right column, allowing a better comparison with the enhanced coherence, the original MSC is scaled, so that the confidence limit, indicated as a horizontal line, is at the same height as the confidence limit of the enhanced MSC.

From the results in Fig. 4 it is clear that the proposed pre-processing indeed amplified the MSC considerably. While the original MSCs in the rows (a)–(c) have their maximums at 0.055, .065 and 0.035, the enhanced MSCs have their maximums at 0.7, 0.69 and 0.52, respectively.

Moreover, in the most cases the enhanced MSCs appear to be more distinct. Comparing left and right column of rows (a)–(d), one can see that the peaks in the enhanced MSCs are slightly more exceeding the confidence limit than the original MSC. In the row (d), where this is the most noticeable, the original MSC is exceeding the confidence limit

[2] That is, the spatially filtered EEG and the rectified EMG is time shifted, pre-processed, and then the coherence is computed.

[3] The time shift should abolish any true coherence and keep only a random one. Therefore, we suggest it to be more than 0.5 s plus the length of a signal segment used in the MSC computation. The value of 0.5 s is based on the results published in [15], where the cortico-muscular cross-correlations were significant only if the mutual time shift was less than 200 ms (we confirmed this result by computing cross-correlations of our EEG–EMG records). Our requirement on the proposed timeshift is actually stronger than in the previous works [16,6], where only a timeshift of the segment length was used.

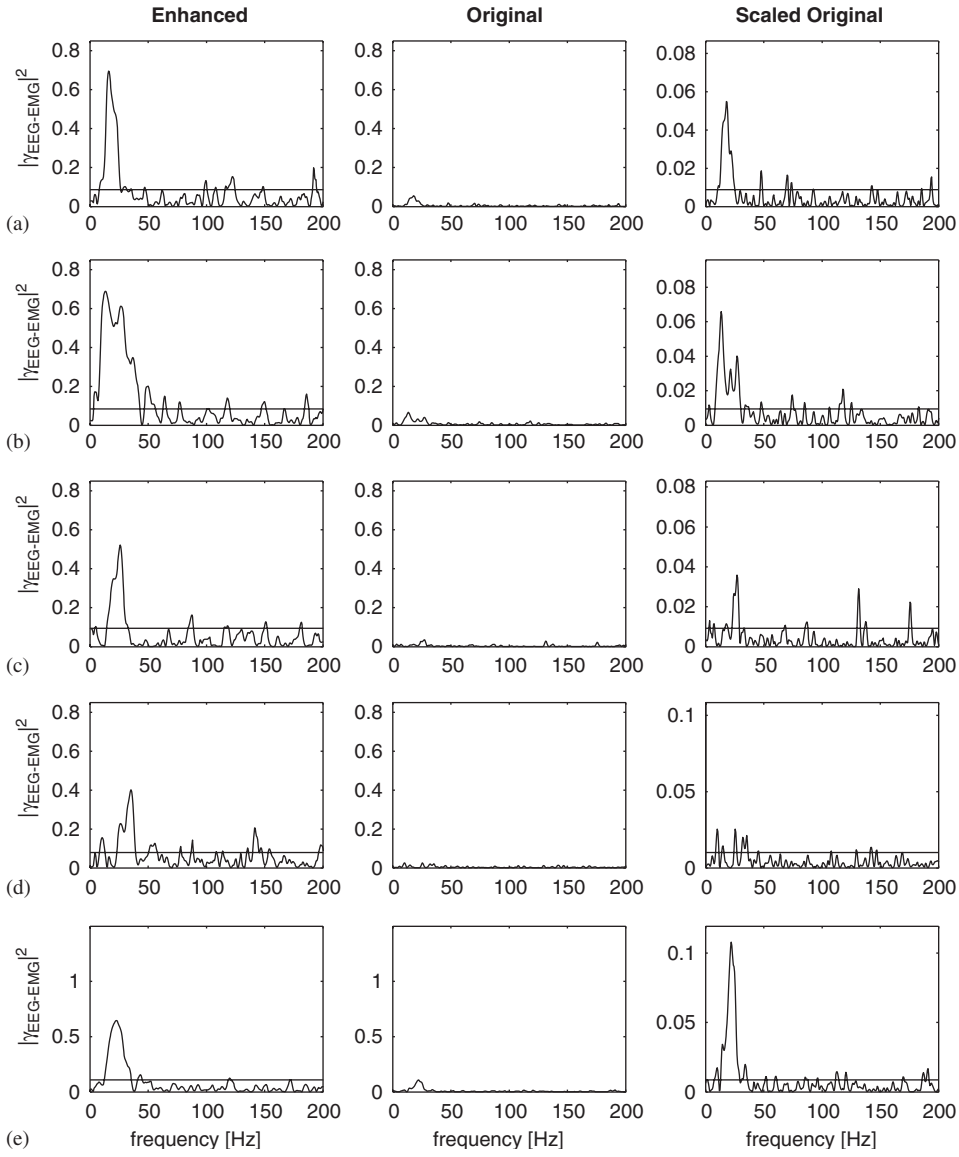

Fig. 4. Examples of EEG–EMG MSCs.

weakly; nevertheless, the enhanced MSC express a more distant peak reaching 0.4.

However, there are some cases where the enhanced MSC does not appear to be more distinct in the mentioned manner. Mostly, these are the cases where the original MSC is, compared to average values in [1,2,4–7], really high (over 0.1), so the further gain in the enhanced MSC is constrained by its upper limit (cannot go over 1). An example of this case is shown in row (e).

Lastly, we present MSCs of uncorrelated EEG and EMG signals. Fig. 5(a) shows an EEG–EMG MSC, where the EEG was recorded over the occipital area (back of the head; a center of vision). Since this area is not involved in muscle control, its EEG record is not related to the EMG of the contracted muscle. In agreement, both original and enhanced MSC confirm that the EEG and EMG records are uncorrelated. Next, in Fig. 5(b), there is an MSC between EEG and EMG signals recorded while the monitored muscle was relaxed (actually, as long as a muscle is not contracted, it does not generate any measurable EMG signal, and its EMG record is essentially composed of noise). In Fig. 5(b)

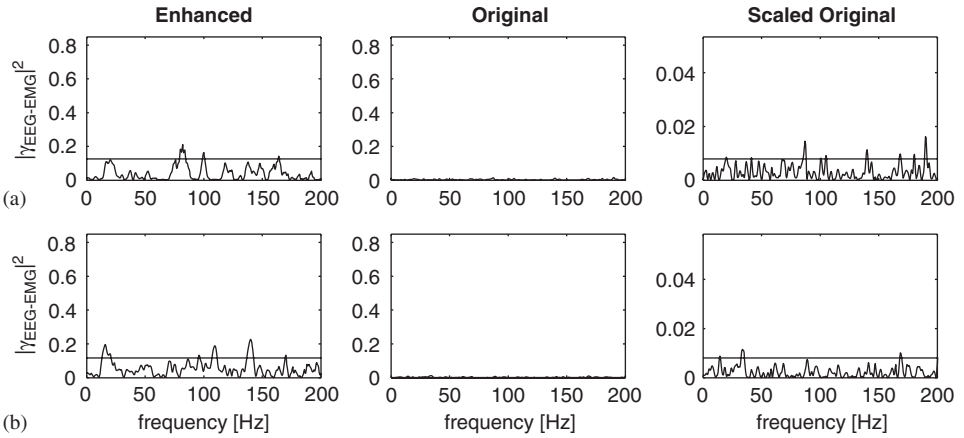

Fig. 5. Examples of EEG–EMG MSCs of uncorrelated EEG and EMG signals.

both enhanced and original MSC show that the EEG and EMG signals, recorded while the monitored muscle was relaxed, are uncorrelated.[4]

Overall, these examples confirm that the enhanced coherence reveals EEG–EMG correlations correctly and in agreement with the physiological expectations.

5. Summary

The paper proposed a new method of the EEG–EMG coherence computation. The performed mathematical analysis showed that if there is any stationary functional connection between EEG and EMG activity, then due to the proposed EEG preprocessing the EEG–EMG MSC can approach unity instead of being below 0.15 as usual. The illustrated practical results showed the EEG–EMG MSC being enhanced from values below 0.1 to values over 0.5. Moreover, an observation was that the enhanced MSC appears to be more distinct than the original one. Overall, the proposed computational method provided a significant boost of the MSC between EEG and EMG signals.[5]

[4]It is possible to observe an occasional exceeding of a confidence limit by the MSCs of uncorrelated signals. This, however, is perfectly normal. Since we use a 95% confidence limit, the MSC of uncorrelated signals will not pass the confidence limit with 95% probability. Thus, on average, 5% of the MSC estimates will exceed the confidence limit (slightly).

[5]All the statements, results and conclusions in this paper hold true (and were tested) even for the case when the electroencephalograph record EEG is replaced by the magnetoencephalograph record MEG.

Acknowledgements

This work has been supported by the research program Transdisciplinary Research in Biomedical Engineering II MSM6840770012 of the Czech Technical University in Prague. Personally, authors would like to thank PhDr. Andrej Stančák for expert technical assistance with EEG and EMG measurements.

Appendix A. Expressing Σ_1 in terms of $u[n]$ and $v[n]$

To express Σ_1 (31) in terms $u[n]$ and $v[n]$, we first substitute (31) with (19)

$$\begin{aligned}\Sigma_1 &= S_v(\Omega)\cdot E[\widehat{H}_l^*(\Omega)\cdot|V_l(\Omega)|^2]\\ &= S_v(\Omega)\cdot E\left[\frac{\widehat{S}_{vul}^*(\Omega)}{S_v(\Omega)}\cdot|V_l(\Omega)|^2\right]\\ &= E[\widehat{S}_{vul}^*(\Omega)\cdot|V_l(\Omega)|^2].\end{aligned}\tag{A.1}$$

Next a substitution of (17), (13) and (10) into the expression (A.1) yields

$$\begin{aligned}&E[\widehat{S}_{vul}^*(\Omega)\cdot|V_l(\Omega)|^2]\\ &\overset{(17)}{\downarrow}\\ &\quad= E[\mathscr{F}\{a_{-k}\widehat{R}_{vul}[-k]\}\cdot|V_l(\Omega)|^2]\\ &\quad= E[A^*(\Omega)*\mathscr{F}\{\widehat{R}_{vul}[-k]\}\cdot|V_l(\Omega)|^2]\overset{(13)}{\downarrow}\\ &\quad= E[A^*(\Omega)*\mathscr{F}\{\widehat{R}_{vun}[-k]\}\cdot|V_l(\Omega)|^2]\overset{(10)}{\downarrow}\end{aligned}$$

$$= E\left[A^*(\Omega) * \mathscr{F}\left\{\sum_{m=n-M}^{n+M} u[m]\cdot v[m+k]\cdot b[n-m]\right\}\cdot |V_l(\Omega)|^2\right]$$

$$= E\left[A^*(\Omega) * \sum_{m=n-M}^{n+M} (u[m]\cdot \mathscr{F}\{v[m+k]\}\cdot b[n-m]\cdot |V_l(\Omega)|^2)\right]$$

$$= A^*(\Omega) * \sum_{m=n-M}^{n+M} (b[n-m]\cdot E[u[m]\cdot \mathscr{F}\{v[m+k]\}\cdot |V_l(\Omega)|^2]). \quad (A.2)$$

This expression can finally be used for further analysis of the coherence function estimate.

Appendix B. Expressing Σ_1 and Σ_2 in terms of $S_{uvl}(\Omega)$, $S_v(\Omega)$, $H(\Omega)$, $e_{S_{uvl}}(\Omega)$ and $e_{Vl}(\Omega)$

To express Σ_1 (31) in terms of these expected values and errors, $\widehat{H}_l^*(\Omega)$ first needs to be expressed using (19), (36), (38) and relation $\widehat{S}_{vul}^*(\Omega) = \widehat{S}_{uvl}(\Omega)$

$$\widehat{H}_l^*(\Omega) = \frac{\widehat{S}_{uvl}(\Omega)}{S_v(\Omega)} = \frac{E[\widehat{S}_{uvl}(\Omega)] + e_{S_{uvl}}(\Omega)}{S_v(\Omega)} = \frac{E[\widehat{S}_{uv}(\Omega)]}{S_v(\Omega)} + \frac{e_{S_{uvl}}(\Omega)}{S_v(\Omega)} = H^*(\Omega) + \frac{e_{S_{uvl}}(\Omega)}{S_v(\Omega)}. \quad (B.1)$$

Next, substituting (B.1) and (37) into (31), and taking into the account that due to the ergodicity of $v[n]$ and $u[n]$ the expected values of the errors $e_{S_{uvl}}(\Omega)$ and $e_{Vl}(\Omega)$ are zero, yields the expression for Σ_1 suitable for further coherence analysis

$$\Sigma_1 = S_v(\Omega)\cdot E\left[\left(H^*(\Omega) + \frac{e_{S_{uvl}}(\Omega)}{S_v(\Omega)}\right)\cdot (S_v(\Omega) + e_{Vl}(\Omega))\right] = S_v^2(\Omega)\cdot H^*(\Omega) + E[e_{S_{uvl}}(\Omega)\cdot e_{Vl}(\Omega)]. \quad (B.2)$$

Now, the expression for Σ_2 (32) will be modified more conveniently. First, $|\widehat{H}_l(\Omega)|^2$ will be substituted with (19), (36) and (38)

$$|\widehat{H}_l(\Omega)|^2 = \frac{|\widehat{S}_{uvl}(\Omega)|^2}{S_v^2(\Omega)} = \frac{(S_{uvl}(\Omega) + e_{S_{uvl}}(\Omega))\cdot (S_{uvl}^*(\Omega) + e_{S_{uvl}}^*(\Omega))}{S_v^2(\Omega)} = \frac{|S_{uv}(\Omega)|^2}{S_v^2(\Omega)} + \frac{S_{uv}(\Omega)\cdot e_{S_{uvl}}^*(\Omega)}{S_v^2(\Omega)} + \frac{S_{uv}^*(\Omega)\cdot e_{S_{uvl}}(\Omega)}{S_v^2(\Omega)} + \frac{|e_{S_{uvl}}(\Omega)|^2}{S_v^2(\Omega)} = |H(\Omega)|^2 + 2\Re\left\{\frac{S_{uv}(\Omega)\cdot e_{S_{uvl}}^*(\Omega)}{S_v^2(\Omega)}\right\} + \frac{|e_{S_{uvl}}(\Omega)|^2}{S_v^2(\Omega)}. \quad (B.3)$$

Next, substitution of (B.3) and (37) into (32) yields

$$\Sigma_2 = S_v^2(\Omega)\cdot E\left[\left(|H(\Omega)|^2 + 2\Re\left\{\frac{S_{uvl}(\Omega)\cdot e_{S_{uvl}}^*(\Omega)}{S_v^2(\Omega)}\right\} + \frac{|e_{S_{uvl}}(\Omega)|^2}{S_v^2(\Omega)}\right)\cdot (S_v(\Omega) + e_{Vl}(\Omega))\right], \quad (B.4)$$

what, taking advantage of the fact that the expected values of errors $e_{S_{uvl}}(\Omega)$ and $e_{Vl}(\Omega)$ are zero, can be simplified into the expression for Σ_2 suitable for further coherence analysis

$$\Sigma_2 = S_v^3(\Omega)\cdot |H(\Omega)|^2 + 2\Re\{S_{uv}(\Omega)E[e_{S_{uvl}}^*(\Omega)\cdot e_{Vl}(\Omega)]\} + S_v(\Omega)E[|e_{S_{uvl}}(\Omega)|^2] + E[e_{Vl}(\Omega)\cdot |e_{S_{uvl}}(\Omega)|^2]. \quad (B.5)$$

(B.6)

Appendix C. EEG and EMG signals

C.1. Electroencephalogram—EEG

A surface EEG is a record of complex activity of a huge number of neurons communicating with each other.

On the cellular level, neurons receive signals through synaptic connections. Excitatory synaptic connections increase their internal potential and inhibitory synaptic connections decrease it. When the internal potential passes a certain threshold a neuron generates (fires) a spiky wave, termed as an action potential. As a result, the internal potential is decreased, and the entire process can be repeated.

Groups of neurons synchronize their activity into an oscillatory pattern. Even though the entire mechanism of these oscillations still remains a bit mysterious, there are some partial explanations. For example, one can imagine the EEG oscillations as an interaction between excitatory and inhibitory neuron pools [18]. The excitatory neuron pools stimulate the inhibitory neurons, which in return depress the excitatory neurons. As the inhibitory neurons are depressed, the excitatory neurons start to fire action potentials again, and the process repeats itself.

The EEG record is a sum of all the electrical activity of the neuron pools. As the number of neurons is huge, the individual action potentials are averaged out, and cannot be observed. But we can still see the oscillatory activity of the neuron pools (Fig. 1). In normal subjects, this oscillatory activity falls in the following frequency bands: 8–13 Hz alpha band (mostly in relaxed state with eyes closed), 15–30 Hz beta band (mostly in awakened or alerted state), 4–8 Hz theta band (mostly in sleep) and <4 Hz delta band (only in deep sleep). Additionally, the power of oscillatory activity usually decreases with increasing frequency. For more information about EEG activity please see [19].

C.2. Electromyogram—EMG

The electromyogram represents a sum of action potentials generated in muscle fibers. The entire process starts when a nerve impulse travelling from a spinal cord arrives to a neuromuscular junction. Through a complex biochemical process it causes an increase of the internal potential of a muscle fiber. When this potential passes a certain threshold the muscle fiber generates a spiky action potential, which means the internal potential is rapidly increased and subsequently decreased (this action potential also evokes a contraction of the muscle fiber). The sum of these spiky action potentials creates a signal measured as the electromyogram (Fig. 1). For more information about electromyogram see [20].

C.3. EEG– EMG coherence

The electrical activity of a contracted muscle was found coherent with the oscillatory activity of neurons in a contralateral primary sensimotor area. A small (about 0.1) but recognizable MSC was observed in the beta (15–30 Hz) and low gamma (30–60 Hz) bands during a moderate muscle contraction [21,9]. In the low gamma band the MEG–EMG MSC was also observed during strong contractions [1]. Occasionally, the EEG–EMG MSC is found in the alpha band (6–12 Hz) [22], though there is some disagreement between the individual findings [9].

Recently, the cortico-muscular coherence analysis is being applied on the study of movement disorders. An abnormal rise of the MSC was reported in the patients suffering from cortical myoclonus [2] and upper limb dystonia [23]. A frequency downshift of MSC was found in the Parkinson patients, where the MSC peak occurs at frequency of the parkinson rest tremor below 10 Hz [9]. Moreover, in the Parkinson patients it is also possible to observe a rise of the MSC at higher frequencies after the application of a treatment [24]. A decrease of MSC is observed in the stroke patients. The cortico-muscular coherence analysis was also used to study essential and exaggerated physiological tremor, even though the published reports [25,26] were contradictory, and failed to distinguish between the individual tremor types [9]. Lastly, one of the future applications of the cortico-muscular coherence can be in the functional neurosurgery, where its possible use would be to find the optimal position of deep brain stimulating electrodes [9].

Appendix D. Computational complexity

In this section we derive computational complexity of the pre-processing formula

$$u'[n] = \sum_{k=-K}^{K} a_k((u[n] \cdot v[n+k]) * b[n])v[n+k]. \tag{D.1}$$

We will assume that the signal length N is much greater than the length of the window $b[n]$, $2M+1$, and the length of the window a_k, $2K+1$.

According to the pre-processing formula, $u[n]$ is first multiplied by $v[n+k]$, which takes N multiplications. Then the result is convolved with $b[n]$, which requires $N \cdot (2M+1)$ multiplications and $N \cdot (2M)$ additions. The result of convolution is multiplied by $v[n-k]$ and a_k, which takes $2N$ multiplications. Finally, this procedure is repeated $2K+1$ times (for $k=-K,\ldots,K$). Thus the total

number of operations approximately is

$$(2K+1)\cdot(N+N\cdot(2M+1)+N\cdot 2M+2N), \tag{D.2}$$

which for $N \gg M$ and $M \gg K$ can be approximated as

$$8KMN. \tag{D.3}$$

The computational complexity can be reduced if the convolution is realized through the Fast Fourier transform. In this case, the convolution requires $N\cdot\log_2(N)$ operations.

Appendix E. Comparison of effects of different windows $b[n]$

In this section we investigate if choosing window $b[n]$ other than Hamming has any affect on the resulting coherence.

We compare enhanced MSCs computed using Hamming, Kaiser and Blackman window. While comparing effects of these windows in the spectral domain of coherence, we want to keep the averaging effects of the correlation estimate (10) unchanged. Therefore, we want the correlation (10) to be estimated with the same variance. We will, therefore, follow the derivation of the variance of a correlation estimate in [13] (formulas (5.66)–(5.69)), but before doing so we will adjust (10) slightly. Namely, to simplify the derivation the summation limits will be taken from $-\infty$ to ∞, while the signals will be considered zero if previously undefined. Additionally, we will use the substitution $z=n-m$

$$\begin{aligned}\widehat{R}_{vun}[k] &= \sum_{m=-\infty}^{\infty} u[m]v[m-k]b[n-m]\\ &= \sum_{z=-\infty}^{\infty} u[n-z]v[n-z-k]b[z].\end{aligned} \tag{E.1}$$

Now, taking the expectation

$$\begin{aligned}R_{uv}[k] &= E[\widehat{R}_{uvn}[k]]\\ &= \sum_{z=-\infty}^{\infty} E[u[n-z]v[n-z-k]]b[z]\\ &= R_{uv}[k]\sum_{z=-\infty}^{\infty} b[z],\end{aligned} \tag{E.2}$$

suggests that

$$\sum_{z=-\infty}^{\infty} b[z]=1. \tag{E.3}$$

This scaling is not needed in the pre-processing, since the MSC is invariant to the scaling; however, it is required in this derivation.

Now, we will analyze the variance of (10)

$$\begin{aligned}\mathrm{Var}[\widehat{R}_{vun}[k]] &= E[\widehat{R}^2_{vun}[k]] - R^2_{vu}[k]\\ &= E\left[\sum_{i,j=-\infty}^{\infty} u[n-i]u[n-j]v[n-i-k]\right.\\ &\quad\left.\times v[n-j-k]b[i]b[j]\right]\\ &\quad - R^2_{vu}[k]\sum_{i,j=-\infty}^{\infty} b[i]b[j].\end{aligned} \tag{E.4}$$

When we restrict $u[v]$ and $v[n]$ to be Gaussian the forth order moment in (E.4) will be given by the second order moments [13]

$$\begin{aligned}&\sum_{i,j=-\infty}^{\infty}(R^2_{vu}[k]+R_u[i-j]R_v[i-j]\\ &\quad + R_{vu}[i-j-k]R_{vu}[i-j+k])b[i]b[j]\\ &\quad - R^2_{vu}[k]\sum_{i,j=-\infty}^{\infty} b[i]b[j].\end{aligned} \tag{E.5}$$

After some simplification and the substitution $\varphi = i-j$ and $\psi = j$ we get

$$\begin{aligned}&\sum_{\varphi,\psi=-\infty}^{\infty}(R_u[\varphi]R_v[\varphi]+R_{vu}[\varphi-k]\\ &\quad\times R_{uv}[\varphi+k])b[\psi+\varphi]b[\psi]\\ &\quad= \sum_{\varphi=-\infty}^{\infty}(R_u[\varphi]R_v[\varphi]+R_{vu}[\varphi-k]\\ &\quad\quad\times R_{uv}[\varphi+k])\sum_{\psi=-\infty}^{\infty} b[\psi+\varphi]b[\psi].\end{aligned} \tag{E.6}$$

Consequently, the variance of correlation (10) will be unchanged if $\sum_{\psi=-\infty}^{\infty} b[\psi+\varphi]b[\psi]$ is kept constant for all the windows $b[n]$. This, of course, is impossible to assure for two arbitrary windows; therefore, we have weakened this requirement, and we require only that

$$\sum_{\psi=-\infty}^{\infty} b[\psi]b[\psi] = \sum_{\psi=-\infty}^{\infty} b^2[\psi] \quad \text{is constant.} \tag{E.7}$$

Even this weakened requirement has provided desired results.

Thus, we adjusted the length of the compared windows so that they were able to meet (E.3) and (E.7). Namely, we used 5000 samples long

Hamming window, 6769 samples long Kaiser window with parameter $\beta = 10$ and 6335 samples long Blackman window.

Each enhanced coherence was computed from two artificially generated signals. These signals were $77 \cdot 10^3$ samples long (the same length as the analyzed EEG signals) with true coherence shown in Fig. 6(a). All the parameters of the pre-processing and coherence computation were the same as the ones used in the section Results. To allow comparison of systematic errors we eliminated random errors by computing the enhanced MSC in 250 trials and taking an average of the results.

The resulting averaged MSCs are shown in Fig. 6. In Fig. 6(b) there is the original MSC estimate. Fig. 6(c)–(e) show the enhanced MSCs estimated using Hamming, Kaiser and Blackman windows, respectively.

To compare the averaged MSCs we computed the differences between them. To evaluate if these differences are of any importance to a single MSC estimate we compared them to a magnitude of random errors represented by the width of MSC confidence intervals $\langle I_{\text{low}}, I_{\text{high}} \rangle$ estimated as

$$I_{\text{low}} = \mu_{0.1} - \overline{|\hat{\gamma}|^2}, \quad I_{\text{high}} = \mu_{0.9} - \overline{|\hat{\gamma}|^2}, \tag{E.8}$$

where $\overline{|\hat{\gamma}|^2}$ denotes the averaged MSC estimate, and $\mu_{0.1}$ and $\mu_{0.9}$ are 10% and 90% quantiles estimated form the individual trials.

The differences between the estimated MSCs in Fig. 6 are shown in Fig. 7. Figs. 7(a), (b) and (c) show the difference between the averaged MSCs computed using the Hamming and Kaiser window, Hamming and Blackman window and Kaiser and Blackman window, respectively.

According to Fig. 7 differences caused by different systematic errors of different windows $b[n]$ are considerably smaller than the width of confidence intervals, which represents the random error. Therefore, we conclude that replacing the Hamming window $b[n]$ with another low leakage window does not have any significant effect on the resulting coherence.

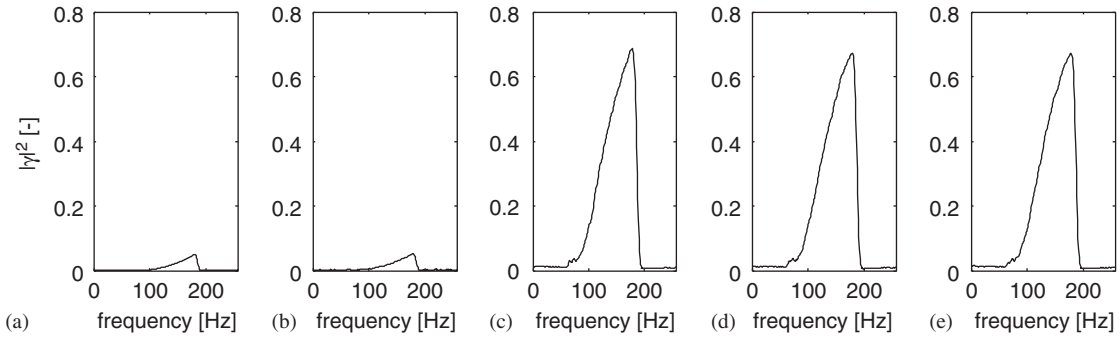

Fig. 6. The comparison of MSCs computed from signals pre-processed with different windows $b[n]$.

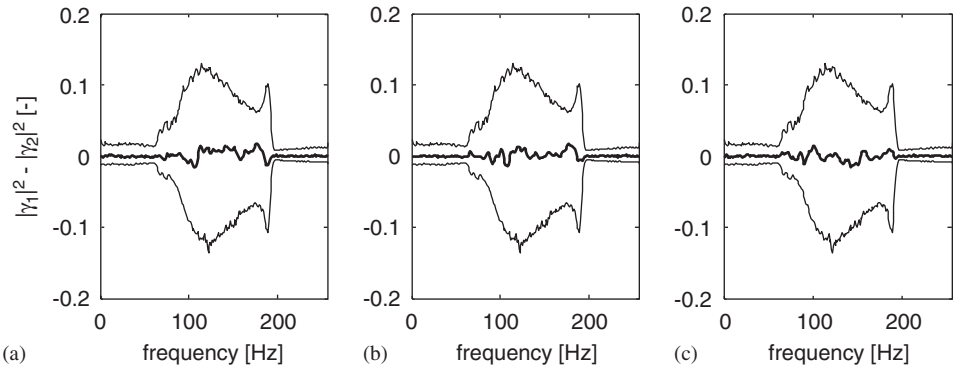

Fig. 7. The differences between averaged MSCs (middle lines) in comparison with the estimated confidence intervals $\langle I_{\text{low}}, I_{\text{high}} \rangle$ (top and bottom lines).

References

[1] P. Brown, S. Salenius, J. Rothwell, R. Hari, Cortical correlate of the Piper rhythm in humans, J. Neurophysiol. 80 (1998) 2911–2917.

[2] B. Conway, D. Halliday, S. Farmer, U. Shahani, P. Maas, A. Weir, J. Rosenberg, Synchronization between motor cortex and spinal motoneuronal pool during the performance of a maintained motor task in man, J. Physiol. 489 (3) (1995) 917–924.

[3] T. Mima, J. Steger, A. Schulman, C. Gerlof, M. Hallett, Electroencephalographic measurement of motor cortex control of muscle activity in humans, Clin. Neurophysiol. 111 (2000) 326–337.

[4] N. Murayama, Y.-Y. Lin, S. Salenius, R. Hari, Oscillatory interaction between human motor cortex and trunk muscles during isometric contraction, Neuroimage 14 (2001) 1206–1213.

[5] J. Rosenberg, A. Amjad, P. Breeze, D. Brillinger, D. Halliday, The Fourier approach to the identification of functional coupling between neuronal spike trains, Prog. Biophys. Mol. Biol. 53 (1989) 1–31.

[6] S. Salenius, K. Portin, M. Kajola, R. Salmelin, R. Hari, Cortical control of human motoneuron firing during isometric contraction, J. Neurophysiol. 77 (1997) 3401–3405.

[7] S. Salenius, R. Salmelin, E.A.C. Neuper, Human cortical 40-Hz rhythm is closely related to EMG rhythmicity, Neurosci. Lett. 21 (1996) 75–78.

[8] P. Brown, Cortical drives to human muscle: Piper and related rhythms, Prog. Neurobiol. 60 (2000) 97–108.

[9] P. Grosse, M. Cassidy, P. Brown, EEG–EMG, MEG–EMG and EMG–EMG frequency analysis: physiological principles and clinical applications, Clin. Neurophysiol. 113 (2002) 1523–1531.

[10] A. Oppenheim, R. Schafer, Discrete-Time Signal Processing, Prentice-Hall, New Jersey, 1999.

[11] G. Jenkins, D. Watts, Spectral Analysis and Its Applications, Holden-Day, San Francisco, CA, 1968.

[12] B. Widrow, S. Stearns, Adaptive Signal Processing, Prentice-Hall, New Jersey, 1985.

[13] J. Bendat, A. Piersol, Random Data: Analysis Measurement Procedures, Wiley, New York, 1971.

[14] J. Bendat, A. Piersol, Engineering Applications of Correlation and Spectral Analysis, Wiley, New York, 1980.

[15] B. Conway, R. Campbell, D. Halliday, Low frequency cortico–muscular coherence during voluntary rapid movements of the wrist joint, Brain Topogr. 16 (4) (2004) 221–224.

[16] J. Gross, P. Tass, S. Salenius, R. Hari, H.-J. Freund, A. Schnitzler, Cortico muscular synchronization during isometric muscle contraction in humans as revealed by magnetoencephalography, J. Physiol. 527 (3) (2000) 623–631.

[17] B. Hjorth, An on-line transformation of EEG scalp potentials into orthogonal source derivations, Electroencephalography Clin. Neurophysiol. 39 (1975) 526–530.

[18] W. Freeman, The physiology of perception, Sci. Am. 264 (2) (1991) 78–85.

[19] E. Niedermeyer, F.L. da Silva, Electroencephalography, Basic Principles, Clinical Applications, and Related Fields, Williams and Wilkins, Baltimore, 1999.

[20] J. Kimura, Electrodiagnosis of neuromuscular disorders, in: W. Bradley, R. Daroff, G. Fenichel, C. Marsden (Eds.), Neurology in Clinical Practice, Butterworth-Heinemann, Boston, 1996, pp. 477–498.

[21] D. Halliday, B. Conway, S. Farmer, J. Rosenberg, Using electroencephalography to study functional coupling between cortical activity and electromyograms during voluntary contractions in humans, Neurosci. Lett. 241 (1998) 5–8.

[22] T. Mima, M. Hallett, Electroencephalographic analysis of cortico-muscular coherence: reference effect volume, conduction and generator mechanism, Clin. Neurophysiol. 110 (1999) 1892–1899.

[23] S. Farmer, G. Sheean, M. Mayston, J. Rothwell, C. Marsden, B. Conway, D. Halliday, J. Rosenberg, J. Stephens, Abnormal motor unit synchronization of antagonist muscles underlies pathological co-contraction in upper limb dystonia, Brain 121 (1998) 801–814.

[24] S. Salenius, S. Avikainen, S. Kaakkola, R. Hari, P. Brown, Defective cortical drive to muscle in Parkinson's disease and its improvement with levodopa, Brain 125 (2002) 491–500.

[25] D. Halliday, B. Conway, S. Farmer, U. Shahnani, A. Russell, J. Rosenberg, Coherence between low-frequency activation of the motor cortex and tremor in patients with essential tremor, Lancet 355 (2000) 1149–1153.

[26] B. Hellwig, S. Häußler, B. Schelter, M. Lauk, B. Guschlbauer, J. Timmer, C. Lücking, Tremor correlated cortical activity in essential tremor, Lancet 357 (2001) 519–523.